c-axis oxygen in copper oxide superconductors

A. Manthiram, X. X. Tang, and J. B. Goodenough
Center for Materials Science and Engineering, The University of Texas at Austin, Austin, Texas 78712
(Received 26 January 1990; revised manuscript received 23 March 1990)

Exploration of the roles of *c*-axis oxygen in the copper-oxide superconductors has revealed a new type of tetragonal-orthorhombic transition in the system $R_{2-z}Ce_zBa_{2-y}L_yCu_3O_{8+x}$ (R = Nd or Gd, L = La or Nd) and one probably due to cluster rotation in fluorinated $La_{2-y}Dy_yCuO_{4-x}F_{2x}$ having the T^* structure with interstitial F ordered in the rocksalt layer. The former is due to *c*-axis ionic displacements that relieve a compressive stress on the (Ba,L)O rocksalt sheets, the latter a tensile stress on the LaO rocksalt sheets. In the $YBa_2Cu_3O_{6+x}$ structure, the *c*-axis oxygen participates in oxygen diffusion in the superconductively inactive layers, they act as gates for stabilizing holes in $Cu(1)O_x$ planes versus CuO_2 sheets, and they modulate the width W of the $\sigma^*_{x^2-y^2}$ conduction band. These modulations are shown to be capable of changing the bandwidth from $W < U$ to $W > U$ and hence to provide a rationalization for the nonsuperconducting metallic copper oxides containing copper in a formal valence state greater than 2+. As modulators of bandwidth, their displacements offer electron-lattice interactions for pairing superconductive holes. In the *n*-type superconductors, interstitial *c*-axis oxygen perturbs the $\sigma^*_{x^2-y^2}$ band so as to introduce localized states at the band edges that suppress superconductivity.

I. INTRODUCTION

The high-T_c copper oxide superconductors all have intergrowth structures consisting of a superconductively active layer of fixed oxygen concentration containing one or more CuO_2 sheets and an inactive layer of variable oxygen concentration. Such a structure introduces anisotropy and the possibility of an internal electric field between layers of opposite charge.[1] In the *p*-type superconductors, a CuO_2 sheet of an active layer interfaces an AO(001) rocksalt sheet in the inactive layer. A measure of the bond-length matching across such an interface is the tolerance factor

$$t = B_{A\text{—O}}/\sqrt{2}B_{\text{Cu—O}} , \tag{1}$$

where the bond lengths $B_{A\text{—O}}$ and $B_{\text{Cu—O}}$ have different thermal expansions, compressibilities, and dependencies on the oxidation state of the CuO_2 sheets. Moreover, the oxygen atoms of the AO rocksalt sheet of the inactive layers are apical, *c*-axis oxygen coordinating the Cu of the CuO_2 sheets of the active layers.

Extensive investigation has also brought out a number of other common features,[2-4] including a mixed-valent compositional range at the narrow-band limit with bandwidth

$$W \approx U > E_p , \tag{2}$$

where U is the intra-atomic correlation energy and E_p is a nonretarded electron-lattice interaction potential for the formation of electron pairs.

In the *p*-type superconductors, oxidation of the antiferromagnetic $(CuO_2)^{2-}$ sheets leads to superconductivity with a critical temperature that varies—for smaller mobile-hole concentrations p—as[5]

$$T_c \sim p/m^* , \tag{3}$$

where m^* is the effective mass of the mobile holes in the CuO_2 sheets. For larger values of p, T_c saturates and then falls to zero. This behavior has been interpreted[6] within the context of a nonretarded electron-lattice pair-binding energy E_p and variable near-neighbor and on-site correlation energies V_c and U. The variation of the correlation energies with local charge-fluctuation and mean Cu—O bond length is implicit in the relation $W \approx U$ of Eq. (2) and is enhanced by a small net energy ΔE for the electron-transfer reaction

$$Cu^{3+} + O^{2-} \rightleftarrows Cu^{2+} + O^- . \tag{4}$$

Moreover, a tolerance factor $t < 1$ removes the Cu-3*d* orbital degeneracy; it stabilizes the Fermi energy in a $\sigma^*_{x^2-y^2}$ band of the CuO_2 sheets (*z* normal to sheet). The width of a $\sigma^*_{x^2-y^2}$ band is determined by the strength of the nearly 180° Cu-O-Cu interactions within a CuO_2 sheet; in the tight-binding approximation,[7]

$$W \approx 8b \sim \varepsilon_\sigma(\lambda_\sigma^2 + \lambda_s^2) , \tag{5}$$

where b is the spin-independent electron-transfer energy integral (resonance integral) for nearest-neighbor copper atoms, ε_σ is a one-electron energy, and the λ_i are covalent-mixing parameters

$$\lambda_i \equiv b_i^{\text{ca}}/\Delta E_i \tag{6}$$

for electron transfer from O-2p_σ or 2*s* orbitals to the empty Cu $3d_{x^2-y^2}$ orbital with a cation-anion (ca) resonance integral b_i^{ca}. W increases while U and V_c decrease sensitively with both a decrease in the mean Cu—O bond length (via b^{ca}) and an increase in p (via the ΔE_i).

All of the *p*-type copper-oxide superconductors have at least one apical oxygen coordinating the Cu atoms of the CuO_2 sheets, and the *n*-type copper-oxide superconductors are perturbed by the introduction of interstitial oxygen at the apical-site positions. In this paper we explore some possible influences of the apical, *c*-axis oxygen on the crystal chemistry and superconductive properties of the copper oxides.

II. BOND-LENGTH MISMATCH

To illustrate the role of the apical oxygen in the relief of bond-length mismatch in the intergrown copper oxides, the systems $R_{2-z}Ce_zBa_{2-y}L_yCu_3O_{8+x}$ (R = Nd or Gd, L = La or Nd) and $La_{2-y}Dy_yCuO_4$ ($0.75 \le y \le 0.9$) have been studied.

A. Experimental

Samples from the first system were prepared[8] by first firing the required quantities of intimately mixed R_2O_3, L_2O_3, $BaCO_3$, and CuO powders at 950 °C for 15 h; the product was ground, pelletized, and refired at 1020 °C for 20 h. The pellet was finally annealed in 1 atm O_2 at 900 °C for 4 h followed by stopping at 700, 500, 350, and 250 °C each for about 12 h before cooling to 100 °C. This procedure was adopted in order to maximize the oxygen content for a 1-atm O_2 anneal.

$La_{2-y}Dy_yCuO_4$ ($0.75 \le y \le 0.9$) samples crystallizing in the T^*-tetragonal structure[9] were obtained by first firing stoichiometric quantities of mixed La_2O_3, Dy_2O_3, and CuO powders at 950 °C for 20 h; the product was ground, pelletized, and refired at 1050 °C for another 20 h. Fluorination of the $y = 0.75$ sample was made by anion exchange. A porous pellet of sample of known weight was placed into a glass tube containing a known quantity of ZnF_2 without making contact with the ZnF_2. The glass tube was then sealed under a vacuum of 0.2 torr and heated at 280 °C for 48 h. During this process, a fraction of the sample oxygen atoms were each exchanged by two fluorine atoms; conversion of the ZnF_2 to ZnO was confirmed by x-ray powder diffraction. The extent of fluorination was controlled by the relative amount of ZnF_2 used. After fluorination, the product was annealed at 400 °C for 24 h in order to achieve chemical homogeneity throughout the sample.

All products were characterized by x-ray powder diffraction with a Philips diffractometer and CuK_α radiation. The oxygen content and the average formal oxidation state of copper were obtained by iodometric titration.[10] All Ce^{4+} ions were assumed to be converted to Ce^{3+} during the titration; this assumption was verified by carrying out the titration under identical conditions with $Ce(NH_4)_4(SO_4)_4 \cdot 2H_2O$. The fluorine content of the fluorinated samples was calculated from the relative quantity of ZnF_2 converted to ZnO. The exchange of two F^- ions for an O^{2-} ion was also verified by iodometric titration, which showed the same formal oxidation state of Cu before and after fluorination.

Thermogravimetric analysis (TGA) was carried out in N_2 and in air with a Perkin-Elmer Series 7 thermal analysis system. Electrical-resistivity measurements were made with a standard four-probe technique on sintered pellets.

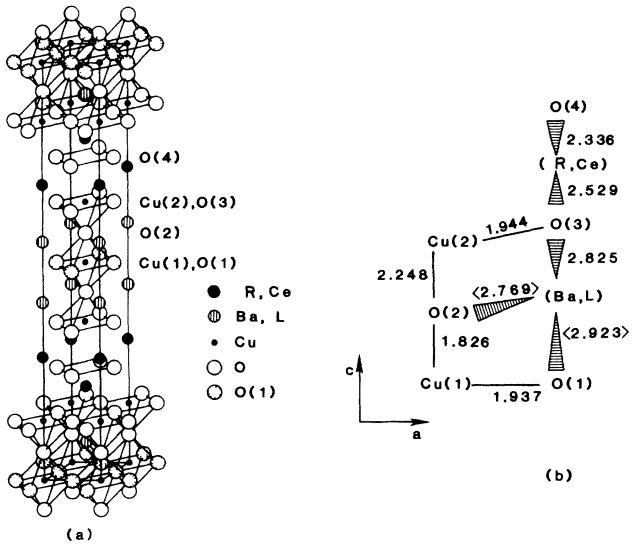

FIG. 1. (a) Crystal structure of $R_{2-z}Ce_zBa_{2-y}L_yCu_3O_{8+x}$ ($R = L$ = rare earth) and (b) bond length values for $R = L$ = Nd, $z = 0.66$ and $y = 0.73$. Adapted from Refs. 8 and 11.

B. $R_{2-z}Ce_zBa_{2-y}L_yCu_3O_{8+x}$

The oxides $R_{2-z}Ce_zBa_{2-y}L_yCu_3O_{8+x}$ (both R and L are rare-earth atoms) have the intergrowth structure illustrated in Fig. 1.[8,11] The half-cell basal-plane sequence along the *c* axis is

$$Cu(1)O_x-(Ba,L)O|Cu(2)O_2-(R,Ce)-O_2-(R,Ce)-Cu(2)O_2|(Ba,L)O-Cu(1)O_x\ , \tag{7}$$

where the superconductively active layer is bounded by the two $Cu(2)O_2$ sheets; the vertical lines represent the interfaces between this active layer and the inactive (Ba,*L*)O-Cu(1)O_x-(Ba,*L*)O layer of variable oxygen content. This structure differs from the familiar $YBa_2Cu_3O_{6+x}$ structure

$$Cu(1)O_x-BaO|Cu(2)O_2-Y-Cu(2)O_2|BaO-Cu(1)O_x \tag{8}$$

by the substitution of the fluorite (R,Ce)-O_2-(R,Ce) block for the Y plane. The interface tolerance factor remains

Eq. (1). (An extensive literature[4] establishes that superconductivity is associated with holes in the CuO_2 sheets of the $YBa_2Cu_3O_{6+x}$ structure; holes trapped out in the $Cu(1)O_x$ planes do not contribute to the superconductivity.)

Sawa *et al.*[8] worked with identical rare-earth ions $R=L=$Nd, Sm, or Eu and observed only tetragonal symmetry for $y=z\approx 0.66$. A high-oxygen-pressure annealing was needed to make these oxides superconductive. A subsequent neutron-diffraction study[11] showed that $x\approx 0.9$ disordered oxygen atoms occupy the $Cu(1)O_x$ planes.

We have extended the investigation of this structure by varying the values of y and z as well as by choosing a different R and L rare-earth atom. Our results show that the variation of y and z is narrow and that the tolerable range of y depends strongly on the size of the L^{3+} ions. For example, with $R=$Nd and $z=0.66$ the formation of a single phase is restricted to the range $0.66\le y\le 1.0$ for $L=$Nd and to $0.8\le y<1.2$ for $L=$La. Similar results were obtained with $R=$Gd and $L=$La, or Nd, but a lower firing temperature ($\sim$960°C) was necessary with $L=$Nd to obtain single-phase samples. With $R=$Nd, $L=$La, and $y=1.0$ single-phase materials were obtained for $0.56\le z\le 0.86$. Thus the ranges of both y and z appear to be restricted.

Figure 2 shows the room-temperature variations with y of lattice parameters, volume, oxygen content, and average formal oxidation state of Cu if all the oxygen are O^{2-} ions for $Nd_{1.34}Ce_{0.66}Ba_{2-y}L_yCu_3O_{8+x}$ ($L=$La and Nd). The average equilibrium oxidation state of copper decreases slightly with increasing y since a $dx/dy<0.5$ is

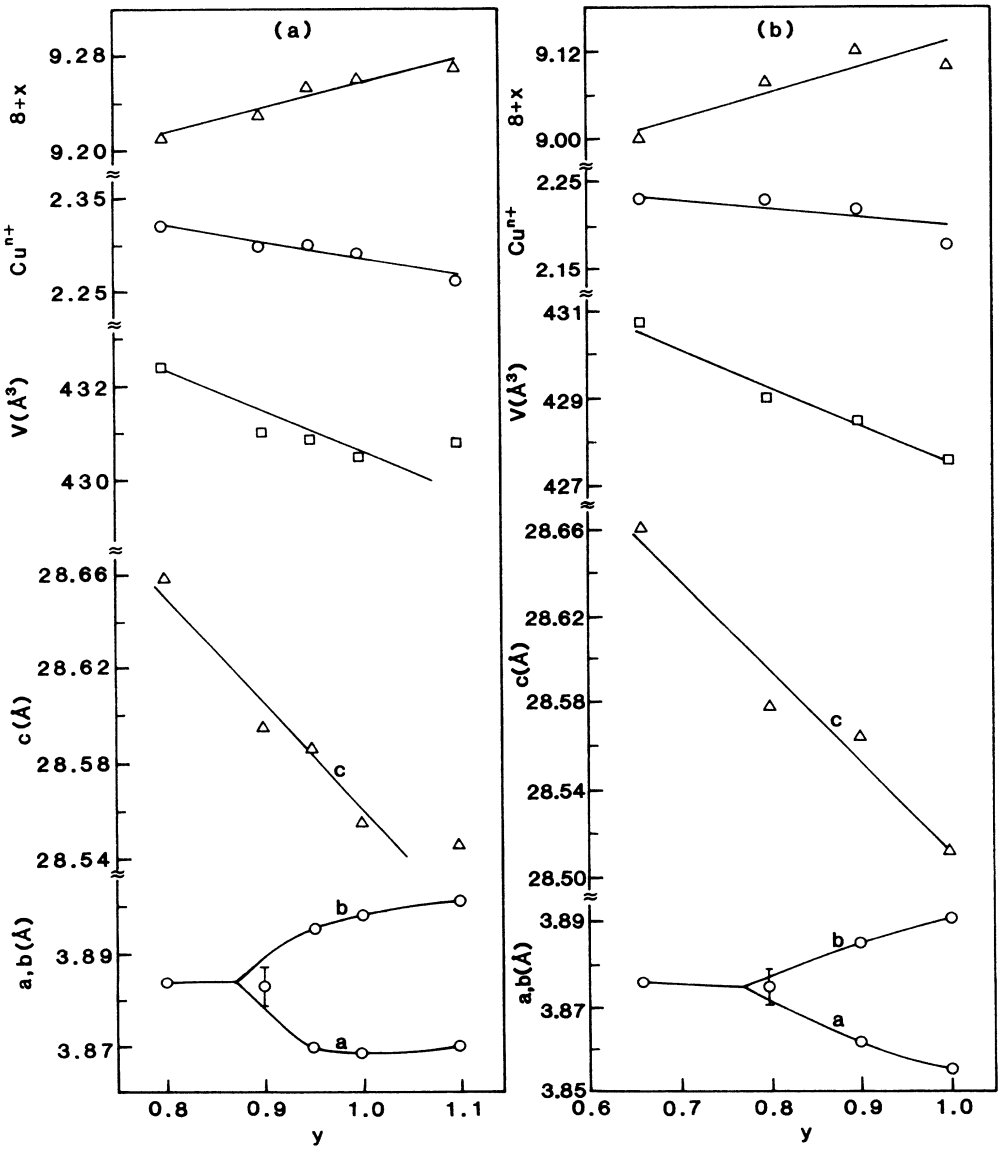

FIG. 2. Variations of lattice parameters, volume, average formal oxidation state of copper Cu^{n+} and oxygen content $(8+x)$ for (a) $Nd_{1.34}Ce_{0.66}Ba_{2-y}La_yCu_3O_{8+x}$ and (b) $Nd_{1.34}Ce_{0.66}Ba_{2-y}Nd_yCu_3O_{8+x}$.

found at 1 atm O_2. Nevertheless, a tetragonal to orthorhombic transition occurs at $y \approx 0.9$ and 0.8 for L = Nd and La, respectively; it is indicated by a splitting or a broadening of such reflections as the (020) and (127), Fig. 3. This distortion is thus seen to depend on the mean size, but not the concentration, of the L cations in the rocksalt planes. The transition temperature T_t crosses room temperature at an average nine-coordinated ionic radius[12] $R_{av} \approx 1.35$ Å. The range of phase stability also appears to be controlled by R_{av} and not by the concentration of L cations in the rocksalt layer. For L = La or Nd, phase stability occurs in the range

$$1.317 \leq R_{av} \leq 1.368 \text{ Å} . \quad (9)$$

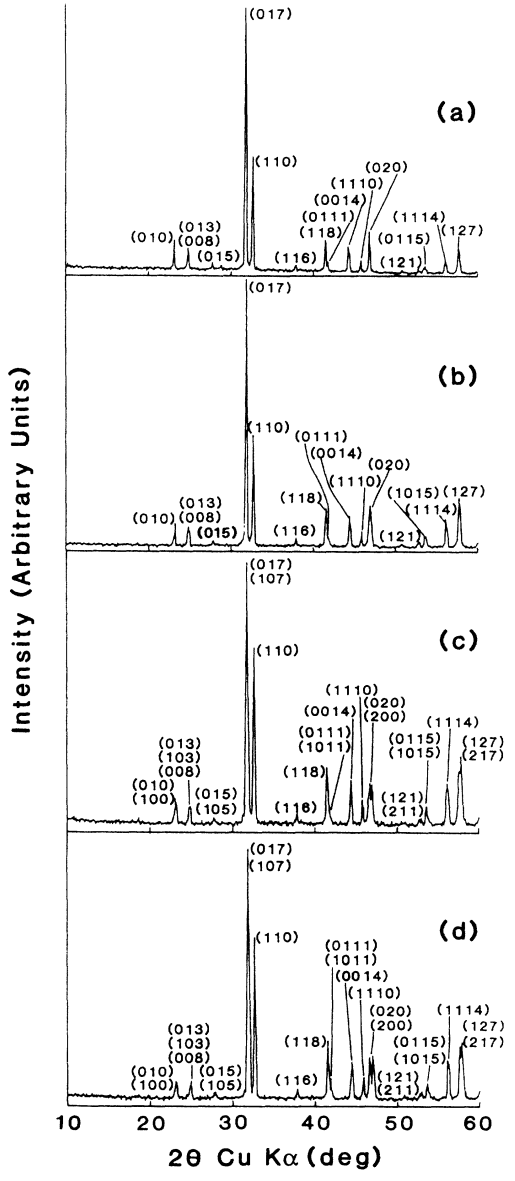

FIG. 3. X-ray powder diffraction patterns of $Nd_{1.34}Ce_{0.66}Ba_{2-y}La_yCu_3O_{8+x}$. (a) $y = 0.8$, (b) $y = 0.9$, (c) $y = 0.95$ and (d) $x = 1.0$.

Thermogravimetric analysis (TGA) of $Nd_{1.34}Ce_{0.66}Ba_{1.1}La_{0.9}Cu_3O_{8+x}$ in N_2 atm and in air at 1 °C/min (Fig. 4) showed, respectively, a loss of about 0.60 and 0.37 oxygen atoms per formula unit between room temperature and 900 °C; above 900 °C in N_2 atm, decomposition of the phase occurs. These compounds lose less oxygen at a given temperature than $YBa_2Cu_3O_{6+x}$. This behavior is characteristic of systems having rare-earth atoms substituted for Ba in the rocksalt layers as in $YBa_{1.5}La_{0.5}Cu_3O_{6+x}$ with $x > 1$.[13] The L^{3+} ions stabilize a-axis oxygen in the $Cu(1)O_x$ planes, and these act as trap sites for mobile holes from the $Cu(2)O_2$ layers.[14] Trapping of holes in the $Cu(1)O_x$ planes renders the oxygen in these planes much less mobile.

In order to determine whether the orthorhombic distortion could, in this case, be due to an unexpected ordering in the $Cu(1)O_x$ planes as along the b axis in orthorhombic $YBa_2Cu_3O_{6+x}$ ($x > 0.35$),[15] the fully oxidized samples were annealed in N_2 in a tubular furnace at 800 °C for 18 h and quenched in N_2. The quenched samples exhibited the orthorhombic distortion at the same values of $y \approx 0.9$ and 0.8 for L = La and Nd, respectively, as the O_2-annealed samples. This observation shows that the orthorhombic distortion observed in this system is not due to either oxygen ordering or to the concentration x of oxygen atoms in the $Cu(1)O_x$ planes; it also rules out any unexpected cation ordering. On the other hand, the results are consistent with a distortion that relieves a tolerance factor $t \neq 1$, Eq. (1).

As pointed out elsewhere,[2] a $t < 1$ places a compressive stress on the CuO_2 sheets and a tensile stress on the rock-

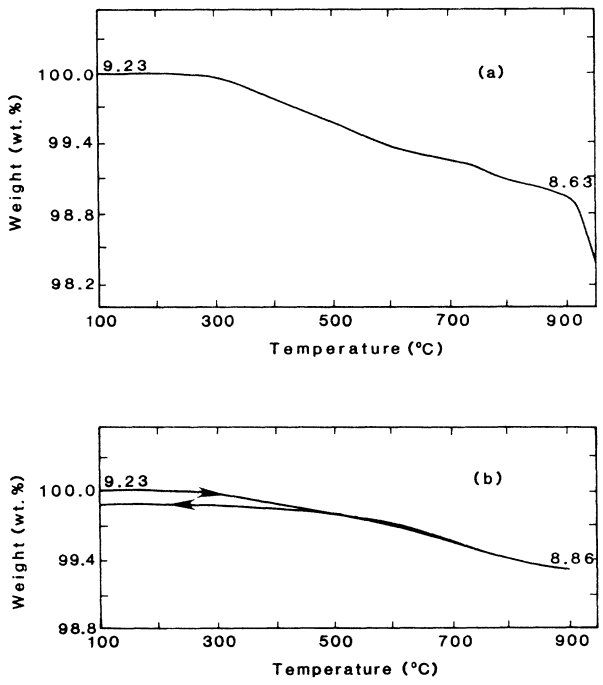

FIG. 4. TGA plots of $Nd_{1.34}Ce_{0.66}Ba_{1.1}La_{0.9}Cu_3O_{9.23}$ at 1 °C/min in (a) N_2 atm and (b) in air. The numbers refer to oxygen content.

salt layers. These stresses increase with decreasing temperature because the thermal expansion of the A—O bonds is larger than that of the Cu—O bonds.

The first relief of the bond-length mismatch is provided by an ordering of the single $3d$ hole per Cu^{2+} ion into a $3d_{x^2-y^2}$ orbital (z normal to CuO_2 sheet, x and y along Cu—O—Cu bonds). In La_2CuO_4 this ordering strongly distorts the CuO_6 octahedra to tetragonal ($c/a>1$) symmetry. The axial ratio of the Cu—O bond lengths is a fair measure of the degree of ordering of the $3d$ hole into $3d_{x^2-y^2}$ versus $3d_{z^2}$, $3d_{z^2-x^2}$, or $3d_{z^2-y^2}$ orbitals.

However, even with ordering of the $3d$ hole into the $3d_{x^2-y^2}$ orbital, a $t<1$ persists in La_2CuO_4. In this case, a second relief of the bond-length mismatch is achieved by the introduction of interstitial oxygen atoms into the rocksalt layers. However, the introduction of interstitial oxygen requires an oxygen mobility, which is not sufficient at lower temperatures where a $t<1$ becomes increasingly important.

At lower temperatures, a third relief mechanism appears; it is a displacive distortion from tetragonal to orthorhombic symmetry consisting of a cooperative tilting of the CuO_6 octahedra about a [110] axis. The tilting bends the Cu—O—Cu bond angles from 180°, thereby relieving the compressive stress on the CuO_2 sheets. This distortion causes a splitting of the (110) reflection of the powder x-ray diffraction pattern.

Unlike the orthorhombic distortion in La_2CuO_{4+x}, there is no splitting of the (110) reflection from the orthorhombic phase of the system $R_{2-z}Ce_zBa_{2-y}L_yCu_3O_{8+x}$ (see Fig. 3). It is therefore necessary to consider some other set of cooperative oxygen displacements to account for the orthorhombic distortion in this system.

Izumi *et al.*[11] have observed, with room-temperature neutron diffraction, a small bending of all the Cu(2)—O—Cu(2) bonds in tetragonal $Nd_{1.34}Ce_{0.66}Ba_{1.27}Nd_{0.73}Cu_3O_{8+x}$ due to a displacement of the bridging oxygen of a CuO_2 sheet toward the smaller (R,Ce) atoms in Fig. 1. A similar O-atom displacement toward the smaller Y atoms is also found in tetragonal $YBa_2Cu_3O_6$. Such a bond bending need not signal that the CuO_2 sheets are under a compressive stress; the tensile stress in the (R,Ce)-O_2-(R,Ce) layer has been relieved by the formation of a fluorite rather than a rocksalt layer. In the case of Nd_2CuO_{4+x}, the smaller tolerance factor relative to that of La_2CuO_{4+x} causes a similar displacement of the c-axis oxygen to give the T'-tetragonal structure with c axis stacking

$$CuO_2|NdO_{x/2}-O_2-NdO_{x/2}|CuO_2\ . \qquad (10)$$

In this case, the Cu—O—Cu bonds remain 180° to lowest temperatures, which is indicative of a possible tensile stress on the CuO_2 planes, at least at higher temperatures. With few, if any, interstitial apical oxygen, this structure lacks the degrees of freedom to adjust to bond-length mismatch found in the T-tetragonal structure of La_2CuO_4, so it is found only for a narrow range R_{av} of the mean rare-earth ionic radius.[2-4] The presence of apical oxygen in the system $R_{2-z}Ce_zBa_{2-y}L_yCu_3O_{8+x}$ introduces a degree of freedom into this system that allows for an adjustment in the CuO_2 layers to relieve bond-length mismatch; it is this adjustment that we believe is responsible for an orthorhombic distortion that does not involve either a tilting of CuO_6 octahedra or an ordering of oxygen atoms in the Cu(1)O_x planes.

Before turning to the specific adjustment, it is worth noting that where the CuO_2 sheets are under a compressive stress, they are readily doped p type, but not n type; removal of antibonding electrons from the $\sigma^*_{x^2-y^2}$ orbitals of the CuO_2 sheets relieves the compressive stress by strengthening the Cu—O bond, whereas the addition of antibonding electrons would enhance it. On the other hand, Nd_2CuO_4 is readily doped n type, but not p type. Thus the relative ease with which the CuO_2 sheets can be doped n type or p type provides a measure of the sign of the internal stresses on the CuO_2 sheets.

In the system $R_{2-z}Ce_zBa_{2-y}L_yCu_3O_{8+x}$, a rocksalt configuration for the 2(R,Ce)O blocks would present a large bond-length mismatch relative to (Ba,La)O(001) rocksalt sheets. This mismatch is partially relieved by formation of fluorite stacking (R,Ce)-O_2-(R,Ce) within the blocks. Further relief is achieved by a bending of the (Ba,La)—O(2)—(Ba,La) bonds in the rocksalt sheet, see Fig. 1(b). However, formation of a (Nd,Ce)-O_2-(Nd,Ce) layer in T'-tetragonal $Nd_{2-y}Ce_yCuO_{4+x}$, stacking sequence (10), appears to place the Cu—O—Cu bonds of a CuO_2 sheet under a slight tensile stress as the sheets are readily doped n type; but this tension refers to Cu—O bonds that are shortened by an ordering of the Cu $3d$ hole into the $3d_{x^2-y^2}$ orbitals in the absence of any apical oxygen atoms. In the system $R_{2-z}Ce_zBa_{2-y}L_yCu_3O_{8+x}$, the Cu(2) atoms of a CuO_2 sheet occupy a square-pyramidal site with a c-axis oxygen forming a 180°Cu(1)—O—Cu(2) bridge. An increasing $3d_{z^2}$ component may be introduced into the $\sigma^*_{x^2-y^2}$ bands with decreasing Cu(2)—O bond length along the c axis.

Nevertheless, the system $R_{2-z}Ce_zBa_{2-y}L_yCu_3O_{8+x}$ remains a semiconductor for $(2x-y-z)\leq 1$ with a shorter Cu(1)—O than Cu(2)—O c-axis bond length. As in the $YBa_{2-y}La_yCu_3O_{6+x}$ system, holes are trapped out of the CuO_2 sheets at five-coordinated Cu(1) atoms in the inactive layer. Oxidation of the CuO_2 sheets to give p-type superconductivity occurs only at oxidation states $(2x\text{-}y\text{-}z)>1$, which corresponds to average formal Cu^{n+} oxidation state $n>2.33$. From Fig. 2(a), an $n=2.33$ is approached in $Nd_{1.34}Ce_{0.66}Ba_{2-y}La_yCu_3O_{8+x}$ at the lower limit of y at 1 atm O_2. A sample of $Nd_{1.44}Ce_{0.56}Ba_{1.2}La_{0.8}Cu_3O_{8+x}$ annealed in 1 atm O_2 has $x\approx 1.16$ which gives an average formal oxidation state of 2.32+ for Cu. A weak semiconductive temperature dependence of the resistivity above a $T_c\approx 40$ K, Fig. 5(a), and a small Meissner signal indicates that the oxygen distribution is not homogeneous; a formal average oxidation state $n>2.33$ per Cu atom may be achieved in a small fraction of the sample. For all values of y in the system $Nd_{1.34}Ce_{0.66}Ba_{2-y}Nd_yCu_3O_{8+x}$ prepared at 1 atm O_2, an $n\leq 2.23$, Fig. 2(b), is found; and all the samples were semiconducting, Fig. 5(b). Sawa *et al.*[8] had to apply a

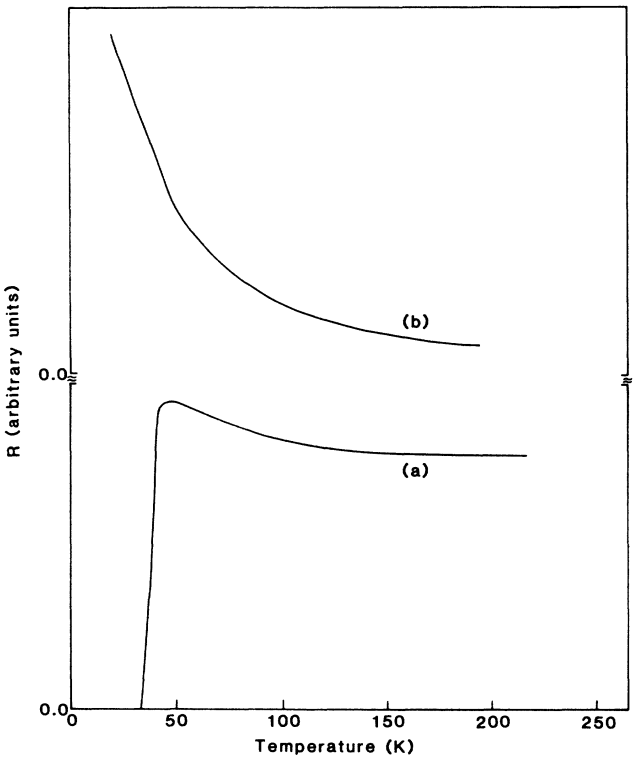

FIG. 5. Variation of resistivity vs temperature for (a) $Nd_{1.44}Ce_{0.56}Ba_{1.2}La_{0.8}Cu_3O_{9.16}$ and (b) $Nd_{1.34}Ce_{0.66}Ba_{1.34}Nd_{0.66}Cu_3O_{9.00}$.

high oxygen pressure to induce superconductivity in the $R=$Nd system; a high oxygen pressure can force an $n>2.33$.

From this analysis, a decrease in R_{av} would reduce bending of the (Ba,L)—O—(Ba,L) bonds in the rocksalt sheets, which in turn reduces the asymmetry of the c axis Cu(2)—O and Cu(1)—O bond lengths. Lessening of the asymmetry need not occur uniformly since a shortening of any Cu(2)-O c-axis bond would be accompanied by a corresponding lengthening of the Cu(2)—O bonds in the CuO_2 sheets so long as the Cu(2)—atom valence state remains formally 2+. A shortening of alternate Cu(2)—O c-axis bond lengths would create orthorhombic symmetry without a tilting of the c-axis O atom from the c axis. It would also create alternate longer and shorter Cu—O bond lengths in the CuO_2 sheets and thus allow adjustments of the bond lengths in the rocksalt layers with a minimal change in the bond bending in the CuO_2 sheets. This hypothesis can be checked by neutron diffraction.

C. The T^* $La_{2-y}Dy_yCuO_{4-x}F_{2x}$ system

The T^*-tetragonal structure[16] combines the T-tetragonal structure of high-temperature La_2CuO_4 with the T'-tetragonal structure of Nd_2CuO_4. The structure, illustrated in Fig. 6, has the following sequence of basal planes on traversing the c axis:

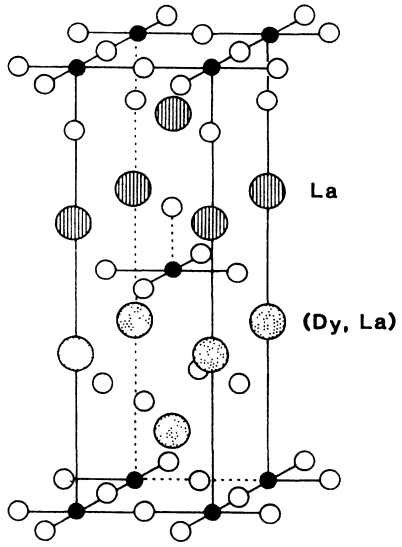

FIG. 6. Crystal structure of T^*-$La_{2-y}Dy_yCuO_4$.

$$CuO_2|AO-AO|CuO_2-A'-O_2-A'-CuO_2|\ , \qquad (11)$$

where $R_{av}(A)>R_{av}(A')$ is needed for bond-length matching. The $La_{2-y}Dy_yCuO_4$ system with $A=$La and $A'=La_{1-y}Dy_y$ was obtained for compositions $0.75\le y\le 0.9$. No orthorhombic distortion has yet been reported for any T^* systems $La_{2-y}R_yCuO_4$ or $Nd_{2-y-z}Ce_ySr_zCuO_4$ ($z>y$), where R is a smaller rare-earth atom.[9,16] We report here the observation of a tetragonal-orthorhombic distortion in a T^* phase that is induced by the replacement of two F^- ions for an O^{2-} ion via anion exchange.

Our initial intent was to introduce n-type conductivity into a T^* phase as had been successfully achieved[17] in the system $Nd_2CuO_{4-x}F_x$. Although n-type T'-$Nd_2CuO_{4-x}F_x$ could be synthesized around 1000 °C by firing a mixture of Nd_2O_3, NdF_3, and CuO, attempts with a similar synthesis of T^*-$La_{2-y}Dy_yCuO_{4-x}F_x$ proved unsuccessful. This finding is consistent with an inability to dope n-type any materials having their CuO_2 sheets under compression. In this compound, the La^{3+} ion is small enough to place the CuO_2 sheets under compression.

We next attempted a low-temperature anion-exchange reaction between ZnF_2 and $La_{1.25}Dy_{0.75}CuO_4$ with varying molar ratios (Table I) to see whether F^- ions could be introduced into the structure. Single-phase compositions $La_{1.25}Dy_{0.75}CuO_{4-x}F_{2x}$ were obtained for $0\le x\le 0.25$ on reaction near 280 °C; above 500 °C phase-disproportionation occurs. Higher molar ratios of ZnF_2 than 1:4 (Table I) produced traces of impurity phases.

The exchange of 2 F^- ions for one O^{2-} ion was established by (a) a quantitative conversion of ZnF_2 to ZnO, (b) a common formal oxidation state of (2.00±0.02)+ for Cu before and after the exchange reaction, (c) an increase in the c axis, (d) a disproportionation of

$La_{2-y}Dy_yCuO_{4-x}F_{2x}$ into T^*-$La_{2-y}Dy_yCuO_4$ and impurity phases such as La_2CuO_4, $(La,Dy)F_3$ and CuO upon heating at 900 °C in an evacuated sealed silica tube—the CuO phase is not visible in the x-ray-diffraction pattern of Fig. 7(d)—and (e) the semiconductive character of $La_{1.25}Dy_{0.75}CuO_{4-x}F_{2x}$.

Figures 7(a)–7(c) show the room-temperature x-ray powder-diffraction patterns for different values of x. A splitting of reflections such as (110), (114), and (123) on fluorination to $x \geq 0.125$ is typical for an orthorhombic distortion like that of room-temperature La_2CuO_4. What distinguishes the tetragonal and orthorhombic phases is the concentration of interstitial F^- ions.

The critical question that remains is the location of the interstitial F^- ions. If they occupy apical, c-axis sites of a fluorite layer

$$CuO_2|LaO-LaO|CuO_2-(La,Dy)F_x-O_{2-2x}F_{2x}-(La,Dy)F_x-CuO_2| \ , \tag{12}$$

then it would be possible to imagine an additional torque on the CuO_5F octahedra to induce a cooperative tilting. However, the fluorite layer is already under compression, and interstitial anions would be incorporated where they can relieve tension. Therefore we should expect the F^- ions to occupy interstitial positions in the rocksalt layers:

$$CuO_2|LaO-F_{2x}-LaO|CuO_2-(La,Dy)-O_{2-2x}F_{2x}-(La,Dy)-CuO_2| \ . \tag{13}$$

Electrostatic interactions would force the anions neighboring an interstitial F^- ion off the c axis, and a rotation of the four displaced c-axis anions about a c axis through their neighboring interstitial anion would relieve the anion-anion electrostatic interactions and produce an orthorhombic distortion of the type observed. Preliminary neutron-diffraction data (P. Lightfoot) on our samples locate the interstitial F^- ions in the interstitial sites of the rocksalt layers, but it could not resolve the origin of the orthorhombic distortion.

III. ROLES IN THE $YBa_2Cu_3O_{6+x}$ STRUCTURE

Extensive studies on systems with the $YBa_2Cu_3O_{6+x}$ structure have identified three other roles played by the c-axis oxygen: participation in oxygen diffusion, gating of holes between active and inactive layers, and modulation of the $\sigma^*_{x^2-y^2}$ band width.

A. Diffusion

We have discussed elsewhere[4,18] the oxygen ordering within $Cu(1)O_x$ planes and the participation of the c-axis oxygen in the oxygen-diffusion process within the inactive layers. We mention it here only for completeness. Interchain ordering at $x=0.5$ and a large energy associated with placement of oxygen on a-axis sites of orthorhombic $YBa_2Cu_3O_{6+x}$, $x>0.5$, forces oxygen insertion to occur down b-axis chains. Diffusion down a b-axis chain through Cu atoms requires the displacement of a c-axis oxygen to a b-axis vacancy by a b-axis oxygen on the opposite side of a Cu atom. Isotope-exchange experiments[19,20] and the loss of c-axis oxygen at higher temperatures[21] confirm the active participation of c-axis oxygen in the diffusion process.

A sample of $YBa_2Cu_3O_{6.70}$—obtained by firing the coprecipitated oxalates at 780 °C followed by an O_2 anneal at 400 °C—is tetragonal and semiconducting;[22] this sample has a much smaller c-axis[22,23] than the orthorhombic superconductive phase with the same oxygen content. The lack of oxygen mobility in this sample has been shown to be associated with trapping of holes at oxygen disordered on a-axis sites in the $Cu(1)O_x$ plane; the reduced c axis suggests the presence of c-axis oxygen vacancies, which would imply that the oxygen disorder includes the c-axis oxygen, and preliminary neutron-diffraction studies[24] confirm this suggestion.

B. Gating

Where the c-axis oxygen bridges—normally asymetrically—a Cu(2) in a CuO_2 sheet and a Cu(1) in the inactive layer, the c-axis oxygen may act as a gate for hole transfer between the Cu(1) and Cu(2) atoms. The stacking sequences (7) and (8) both have c-axis Cu(2)—O—Cu(1) bonding. Displacement of a c-axis oxygen toward one bridged Cu and away from the other changes the relative strengths of the Cu—O covalent mixing at the two Cu atoms. The shorter a Cu—O bond length, the greater is λ_σ and the more unstable are the antibonding states associated with a Cu-3d parentage. Therefore shortening of a c-axis Cu—O bond on one side of a bridge and lengthening of the bond on the opposite side of the bridge may shift the relative energies at the two copper atoms so as to effect a hole transfer. Cava *et al.*[25] were the first to call attention to a pronounced shortening of the c-axis Cu(2)—O bond in $YBa_2Cu_3O_{6+x}$ on passing from the tetragonal, antiferromagnetic phase ($x<0.3$) with only Cu^{2+} ions in the CuO_2 sheet to the superconductive orthorhombic phase ($x>0.4$) having mobile holes in the CuO_2 sheets.

Figure 8 displays the room-temperature variation with x of the lattice parameters and of several mean bond lengths in well-ordered samples of $YBa_2Cu_3O_{6+x}$; the data are from powder neutron-diffraction experiments of Jorgensen *et al.*[26] A step in T_c versus x in the interval $0.5<x<0.75$ is characteristic of interchain oxygen ordering in the $Cu(1)O_x$ planes with oxidation of primarily $Cu(1)^+$ to $Cu(1)^{2+}$ in the partially occupied chains in this compositional range.[18] It is noteworthy that there is no corresponding step in the lattice-parameter or bond-length variations with x. However, the data clearly show an abrupt shift of the c-axis O(4) atoms away from the

TABLE I. Anion exchange products[a] and lattice parameters.

Starting composition	Ratio of starting material: ZnF_2	Product composition	Lattice parameters (Å) a	b	c	Volume (Å^3)
$La_{1.25}Dy_{0.75}CuO_4$			3.870(2)	3.870(2)	12.450(4)	186.2
$La_{1.25}Dy_{0.75}CuO_4$	8:1	$La_{1.25}Dy_{0.75}CuO_{3.875}F_{0.25}$	3.877(3)[b]	3.877(3)	12.480(5)	187.6
$La_{1.25}Dy_{0.75}CuO_4$	4:1	$La_{1.25}Dy_{0.75}CuO_{3.75}F_{0.5}$	5.463(3)	5.510(3)	12.487(4)	375.8
$La_{1.25}Dy_{0.75}CuO_4$	3:1	$La_{1.25}Dy_{0.75}CuO_{4-x}F_{2x}$ ($x \geq 0.25$) + $(La,Dy)F_3$	5.464(2)	5.515(2)	12.488(4)	376.3

[a]All samples have an average oxidation state of $(2.00 \pm 0.01)+$ for Cu.

[b]Pseudotetragonal parameters; orthorhombic parameter could not be refined because of broadening or weak splitting of reflections such as (020) and (024).

Cu(1) toward the Cu(2) atoms on increasing x through the tetragonal-orthorhombic transition near $x = 0.35$. Within the orthorhombic phase, this shift is nearly linear; it is apparently dominated by a coulombic repulsion between the c-axis oxygen and the oxygen of a $Cu(1)O_x$

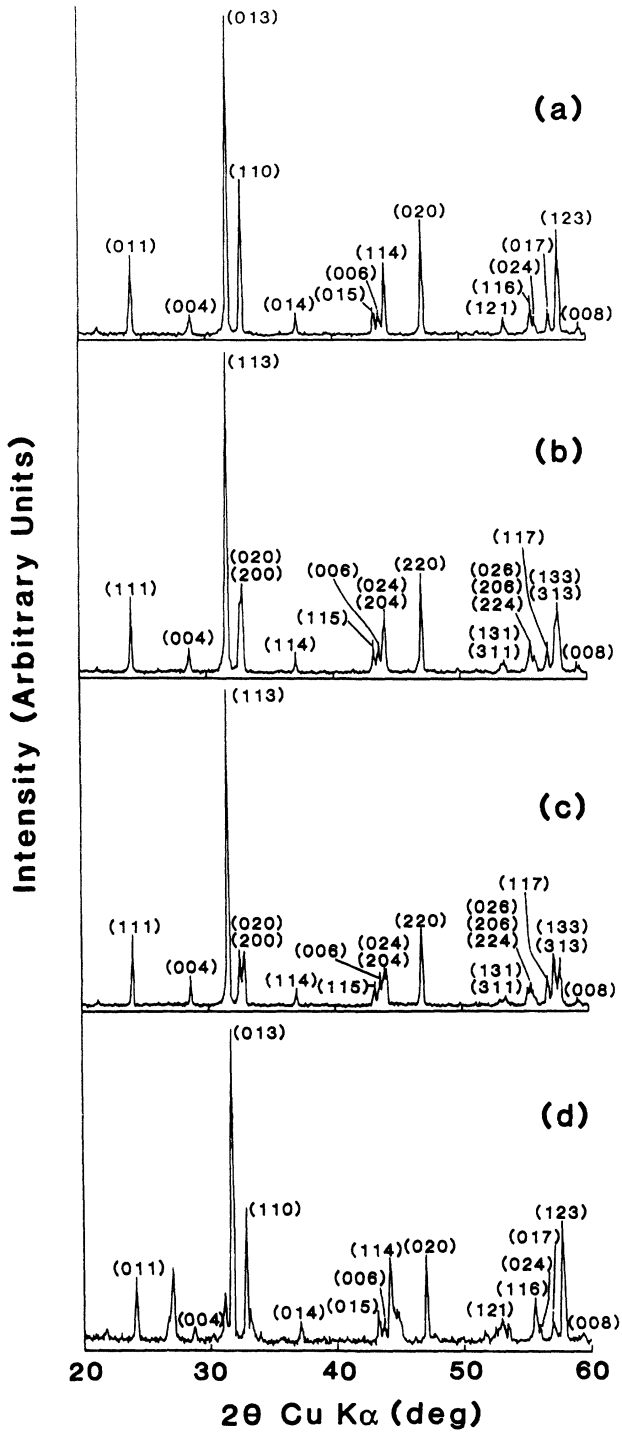

FIG. 7. X-ray powder diffraction patterns of $La_{1.25}Dy_{0.75}CuO_{4-x}F_{2x}$: (a) $x = 0.0$, (b) $x = 0.125$, (c) $x = 0.25$ and (d) sample $x = 0.25$ after annealing in evacuated sealed silica tube at 900 °C for 10 h. The unindexed lines in (d) refer to impurity phases such as $(La,Dy)F_3$ and La_2CuO_4.

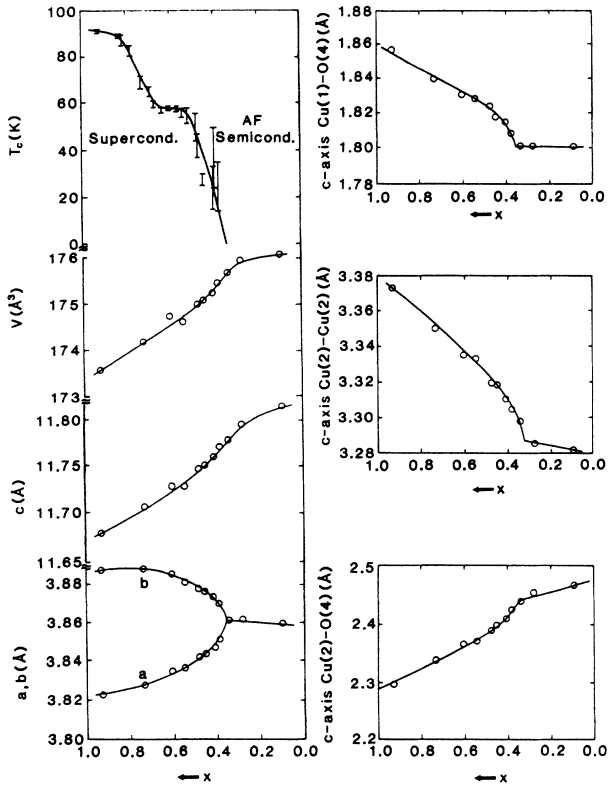

FIG. 8. Variations of lattice parameters, volume, T_c and c-axis Cu-O and Cu-Cu distances with x in $YBa_2Cu_3O_{6+x}$. Adapted from Jorgensen *et al.* (Ref. 26).

plane, which increases with x. Once the Cu(2)—O c-axis bond length is short enough to favor oxidation of $Cu(2)^{2+}$, the Cu(1)—O c-axis bond length is not constrained to be short.

C. Band-width modulation

The tetragonal-orthorhombic transition in the $YBa_2Cu_3O_{6+x}$ system is also a transition from an antiferromagnetic, small-polaron conductor to a superconductor. A change from small-polaron to itinerant-electron behavior and a decrease in volume are indicative of a sharp increase in the bandwidth W of the $\sigma^*_{x^2-y^2}$ band even though the mean Cu—O bond length within a CuO_2 sheet shows little, if any, contraction. From Eq. (5) an increase in W means an increase in λ_σ and λ_s; but a constant Cu—O distance means little change in b^{ca}, which implies that the increase in W is due to a decrease in the electron-transfer energy ΔE. A decrease in the c-axis Cu—O distance would raise the $3d_{z^2}$ energies relative to the $3d^*_{x^2-y^2}$ energies, but its effect on the partially filled $\sigma^*_{x^2-y^2}$ would be relatively small. (We neglect the π^* bands, but the π_{yz} and π_{zx} would be raised relative to the π^*_{xy} at the top of the π^* bands.) On the other hand, a marked increase in the Coulombic repulsion between c-axis and basal-plane oxide ions significantly lowers the Madelung stabilization of the O $2p$ orbitals relative to the Cu $3d$ orbitals, thereby lowering ΔE and increasing W according to Eqs. (5) and (6).

IV. OTHER COPPER OXIDES

A. Band-width modulation

Correlation of an increasing bandwidth with a decreasing c-axis Cu—O bond length at the copper of the CuO_2 sheets is also found in other copper oxides. For example, the antiferromagnetic compositions of the systems $Bi_2(Sr_{1.5}Ca_{0.5})Ca_{1-y}Y_yCu_2O_{8+x}$ and $Bi_{2-z}Pb_z(Sr_{1.5}Ca_{0.5})Ca_{1-y}Y_yCu_2O_{8+x}$ with $y=z$ have a larger c axis, which is compatible with a larger c axis Cu(2)—O distance, than is anticipated from an extrapolation from the superconductive to the antiferromagnetic compositions in accordance with Vegard's law (Figs. 9 and 10).[27] Moreover, an increase in T_c with hydrostatic pressure in $YBa_2Cu_4O_8$ has recently been found[28] to correlate with a decrease in the c axis and the apical Cu(2)—O distance. Finally, the change from normal metal to superconductor with decreasing oxidation (increasing x) in $Tl_{2-y}Ba_2CuO_{6-x}$ (Refs. 29 and 30) is ac-

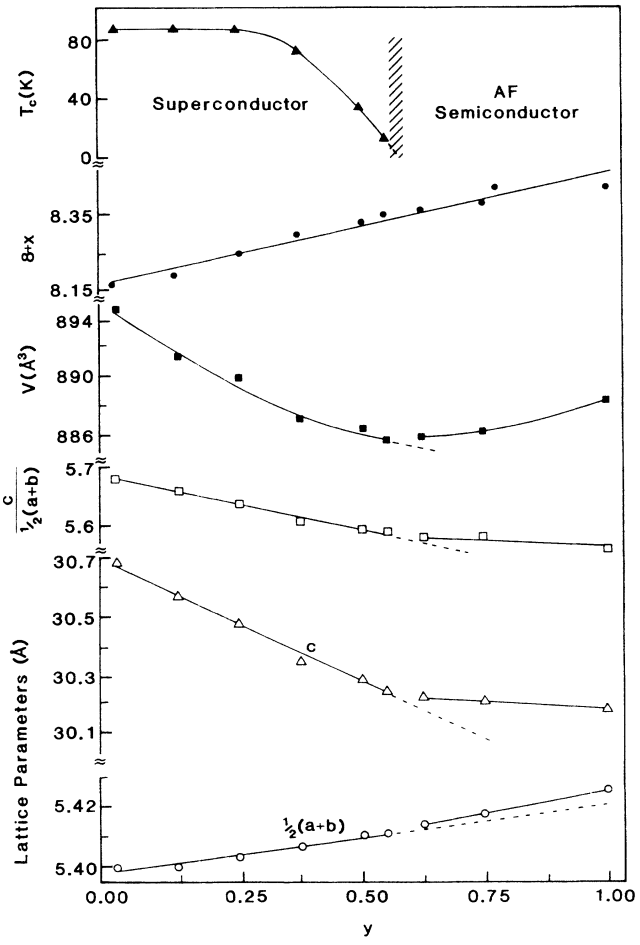

FIG. 9. Variations of lattice parameters, volume, oxygen content $(8+x)$ and T_c with y for $Bi_2(Sr_{1.5}Ca_{0.5})Ca_{1-y}Y_yCu_2O_{8+x}$.

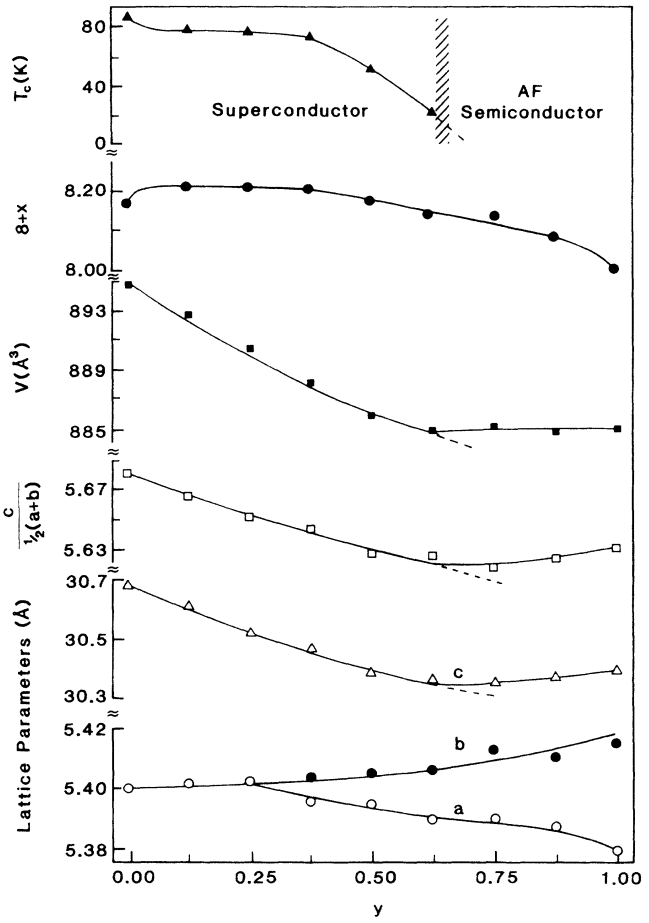

FIG. 10. Variations of lattice parameters, volume, oxygen content $(8+x)$ and T_c with y for $Bi_{2-z}Pb_z(Sr_{1.5}Ca_{0.5})Ca_{1-y}Y_yCu_2O_{8+x}$ with $z=y$.

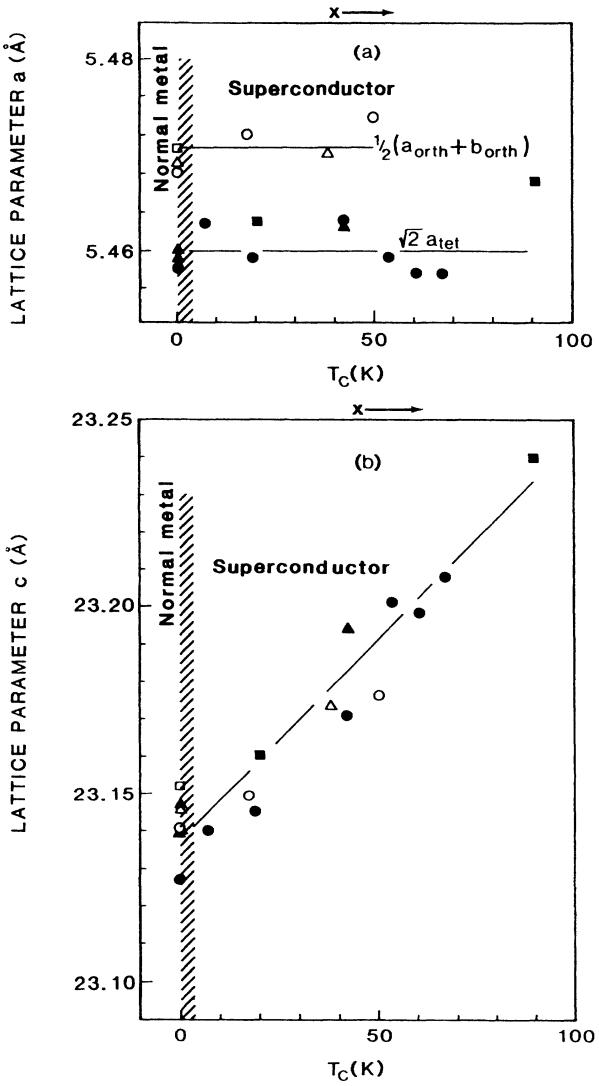

FIG. 11. Variations of (a) a and b and (b) c parameters with T_c for $Tl_{2-y}Ba_2CuO_{6-x}$. Adapted from Ref. 29.

companied by an increase in the c axis; and T_c increases linearly with the c-axis in the superconductive region (Fig. 11). In this latter system, T_c decreases with increasing oxidation state and bandwidth.

In all of the preceding cases, superconductivity correlates with a c-axis and/or an apical Cu—O distance that is intermediate in magnitude between a larger value in the antiferromagnetic phase at smaller oxidation of the CuO_2 sheets and a smaller value in a normal-metal phase at larger oxidation. The apical Cu—O bond length thus appears to modulate significantly the width of the conduction band from a $W < U$ (antiferromagnetic phase) for a larger bond length to $W > U$ (normal-metal phase) for a smaller c-axis Cu—O bond length. We have emphasized elsewhere[6,31] for p-type superconductors, the possible role in superconductive pairing of displacements along the c-axis of in-plane oxygen in Cu—O—Cu bonds bent from 180°; it is clear that c-axis displacements of the apical oxygen can play a similar role.

B. Metallic copper oxides

There are a few copper-oxide systems such as $La_{2-y}Sr_{1+y}Cu_2O_{6+x}$, $La_4BaCu_5O_{13}$, and $La_5SrCu_6O_{15}$ that are metallic down to 4 K, but not superconductive;[32–34] they have a formal mean oxidation state of Cu in excess of 2+ like the p-type superconductors. In $La_{2-y}Sr_{1+y}Cu_2O_{6+x}$, the excess x oxygen atoms ($x \approx 0.25$ for $y=0.15$) occupy the c-axis positions of the (La,Sr) planes between the two CuO_2 sheets; these make two short c-axis Cu—O bonds. In the other two compounds, some of the copper atoms are octahedrally coordinated with a short c-axis Cu—O bond. A shorter Cu—O distance is associated with a $W > U$ in all of these systems; and the small correlation energies implicit in $W > U$ appear to be associated with a suppression of superconductivity.[6,31] The limiting case of these systems is the rhombohedral perovskite $LaCuO_3$, which is a normal metal[35] with all the Cu atoms in octahedral coordination.

C. Anderson localization

Superconductivity is found in copper oxides containing CuO_2 sheets with a $\sigma^*_{x^2-y^2}$ conduction band at the

narrow-band limit. In this limit, relatively small perturbations of the band can introduce localized states at the edges of the band. If the Fermi energy lies within the tail of localized states (above a mobility edge in p-type conductors or below in n-type conductors), conduction is by variable-range hopping and superconductivity is suppressed. In $PrBa_2Cu_3O_{6+x}$, the Pr^{3+}:$4f^2$ configuration has an energy close enough to E_F to perturb the conduction-band states near E_F sufficiently to destroy superconductivity.[36,37] From this reasoning, it follows that where there are interstitial anions randomly distributed in c-axis sites, they should perturb the $\sigma^*_{x^2-y^2}$ bands so as to introduce a mobility edge that could penetrate deeply into the conduction band.

This situation appears to be illustrated by the n-type superconductors $R_{2-y}M_yCuO_{4+x}$ with $0.15<y<0.18$, R=Pr-Eu, and M=Ce or Th, all of which have the T'-tetragonal structure for the stoichiometric compositions $x=0$.[38-40] Synthesis of these phases at ca. 1050 °C in air followed by furnace cooling introduces excess oxygen ($x\approx0.04$) into the interstitial c-axis positions.[41,42] The presence of randomly positioned c-axis oxygen not only reduces the electron concentration n; it also makes the compositions semiconductors with a conductivity typical of that found for variable-range hopping, Fig. 12(a). TGA indicates that the excess oxygen atoms are lost above ~700 °C in N_2. Annealing of these phases in an inert atmosphere is necessary to convert these oxides to normal metals exhibiting n-type superconductivity at lowest temperatures. The solid-solution range for $Nd_{2-y}Ce_yCuO_4$ is limited to $y\leq0.2$. We have found that the upper limit can be increased to $y=0.25$ by increasing the a parameter as in $La_{1.3}Nd_{0.45}Ce_{0.25}CuO_{4+x}$. Significantly, $La_{1.3}Nd_{0.45}Ce_{0.25}CuO_{4+x}$, after an anneal in O_2 at 700 down to 250 °C followed by slow cooling in the furnace is a semiconductor, Fig. 12(a), with $x=0.04$ even though it has about 0.17 electrons/formula unit as in the n-type superconductors; an anneal in 1 atm N_2 at 900 °C gives $x=0.00$ and normal metallic behavior, Fig. 12(b), with a higher electron concentration $n=0.25$.

V. CONCLUSIONS

The c-axis oxygen have been shown to play several key roles in the copper-oxide superconductors. These roles include the following. (1) Relief of bond-length mismatch between the superconductively active and inactive layers by (a) cooperative c-axis displacements where the rocksalt layers are under compression as in $R_{2-z}Ce_zBa_{2-y}L_yCu_3O_{8+x}$ and (b) insertion of interstitial anions into the rocksalt layers where they are under tension and the CuO_2 sheets are under compression as in

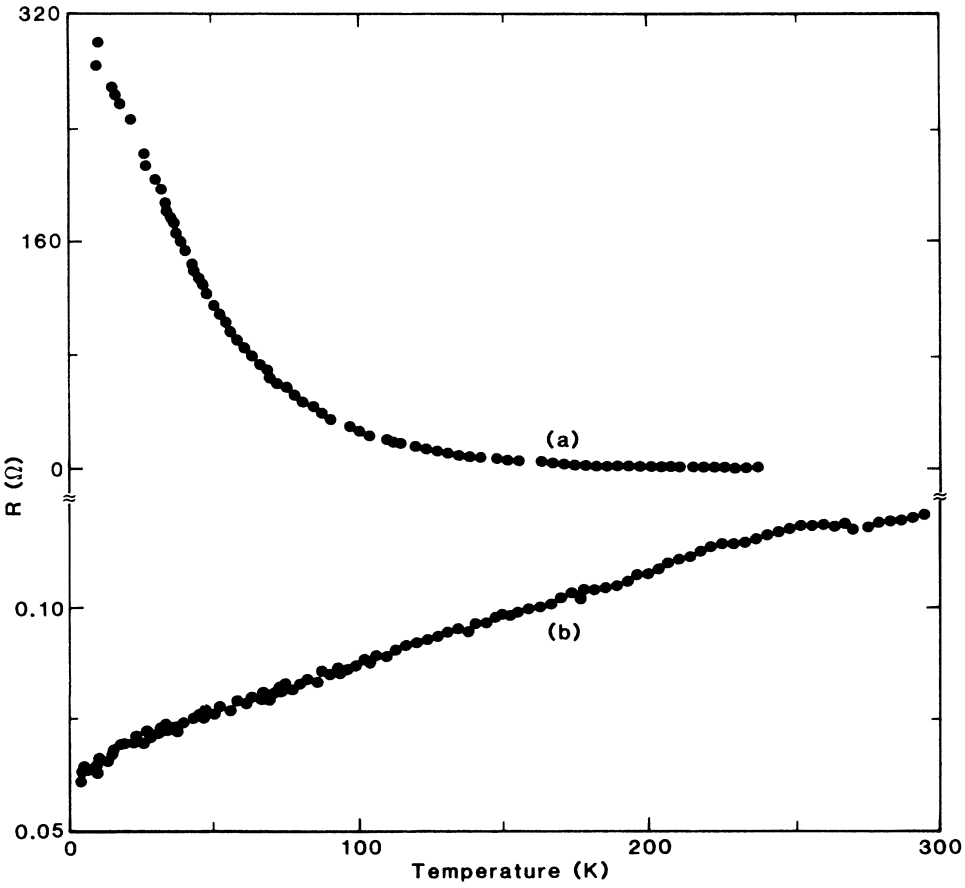

FIG. 12. Resistivity vs temperature for $La_{1.3}Nd_{0.45}Ce_{0.25}CuO_{4+x}$: (a) $x=0.04$ and (b) $x=0.0$.

La_2CuO_4 or in T^*-$La_{2-y}Dy_yCuO_{4-x}F_{2x}$. (2) Participation in oxygen diffusion in the inactive layers. (3) Gating of mobile charge carriers between Cu in the active and inactive layers. (4) Modulation of the $\sigma^*_{x^2-y^2}$ bandwidth in the CuO_2 sheets, which makes its c-axis displacements candidate motions for the trapping of superconductive electron (hole) pairs by strong electron-lattice interactions. (5) Perturbations of the $\sigma^*_{x^2-y^2}$ bands that introduce Anderson-localized states at the band edges—or deeply into the band—where interstitial c-axis oxygen are randomly positioned.

ACKNOWLEDGMENTS

We gratefully acknowledge support for this research by the Texas Advanced Research Program Grant No. 4257 and the Robert A. Welch Foundation, Houston, TX.

[1]J. B. Goodenough, J. Less Common Met. **116**, 83 (1986).
[2]J. B. Goodenough, Supercond. Sci. Technol. **3**, 26 (1990).
[3]J. B. Goodenough and A. Manthiram, in *Studies of High Temperature Superconductors,* edited by A. V. Narlikar (Nova Science, New York, in press), Vol. 5.
[4]A. Manthiram and J. B. Goodenough, in *Advances in the Synthesis and Reactivity of Solids,* edited by T. E. Mallouk (Jai, Greenwich, in press), Vol. 1.
[5]Y. J. Uemura *et al.*, Phys. Rev. Lett. **62**, 2317 (1989).
[6]J. B. Goodenough and J. Zhou, Phys. Rev. B (to be published).
[7]J. B. Goodenough, Prog. Solid State Chem. **5**, 145 (1971).
[8]H. Sawa, K. Obara, J. Akimitsu, Y. Matsui, and S. Horiuchi, J. Phys. Soc. Jpn. **58**, 2252 (1989).
[9]S. W. Cheong, Z. Fisk, J. D. Thompson, and R. B. Schwarz, Physica C **159**, 407 (1989).
[10]A. Manthiram, J. S. Swinnea, Z. T. Sui, H. Steinfink, and J. B. Goodenough, J. Am. Chem. Soc. **109**, 6667 (1987).
[11]F. Izumi, H. Kito, H. Sawa, J. Akimitsu, and H. Asano, Physica C **160**, 235 (1989).
[12]R. D. Shannon, Acta Crystallogr. A **32**, 751 (1976).
[13]A. Manthiram, X. X. Tang, and J. B. Goodenough, Phys. Rev. B **37**, 3734 (1988).
[14]Y. Dai, A. Manthiram, A. Campion, and J. B. Goodenough, Phys. Rev. B **38**, 5091 (1988).
[15]J. D. Jorgensen, B. W. Veal, W. K. Kwok, G. W. Crabtree, A. Umezawa, L. J. Nowicki, and A. P. Paulikas, Phys. Rev. B **36**, 5731 (1987).
[16]H. Sawa, S. Suzuki, M. Watanabe, J. Akimitsu, H. Matsubara, H. Watabe, S. Uchida, K. Kokusho, H. Asana, F. Izumi, and E. Takayama-Muromachi, Nature **337**, 347 (1989).
[17]A. C. W. P. James, S. M. Zahurak, and D. W. Murphy, Nature **338**, 240 (1989).
[18]C. J. Hou, A. Manthiram, L. Rabenberg, and J. B. Goodenough, J. Mater. Res. **5**, 9 (1990).
[19]W. K. Ham, S. W. Keller, J. N. Michaels, A. M. Stacy, D. Krillov, D. T. Hodul, and R. H. Flemming, J. Mater. Res. **4**, 504 (1989).
[20]M. Cardona, R. Liu, C. Thomsen, W. Kress, S. Schonherr, M. Bauer, L. Genzel, and W. Konig, Solid State Commun. **67**, 789 (1988).
[21]C. Namgung, J. T. S. Irvine, J. S. Binks, and A. R. West, Supercond. Sci. Technol. **1**, 169 (1988); J. D. Jorgensen, H. Shaked, D. G. Hinks, B. Dabrowski, B. W. Veal, A. P. Paulikas, L. J. Nowicki, G. W. Crabtree, W. K. Kwok, L. H. Nimez, and H. Claus, Physica C **153-155**, 578 (1988).
[22]A. Manthiram and J. B. Goodenough, Nature **329**, 701 (1987).
[23]J. B. Goodenough and A. Manthiram, Physica C **157**, 439 (1989).
[24]J. D. Jorgensen, A. Manthiram, and J. B. Goodenough (unpublished).
[25]R. J. Cava, B. Batlogg, K. M. Rabe, E. A. Rietman, P. K. Gallagher, and L. W. Rupp, Jr., Physica C **156**, 523 (1988).
[26]J. D. Jorgensen, B. W. Veal, A. P. Paulikas, L. J. Nowicki, G. W. Crabtree, H. Claus, and W. K. Kwok, Phys. Rev. B **41**, 1863 (1990).
[27]A. Manthiram and J. B. Goodenough, Appl. Phys. Lett. **53**, 420 (1988); **53**, 2695 (1988).
[28]E. Kaldis, D. Fischer, A. W. Hewat, E. A. Hewat, J. Karpinski, and S. Rusiecki, Physica C **159**, 668 (1989).
[29]Y. Shimakawa, Y. Kubo, T. Manako, T. Satoh, S. Iijima, T. Ichihasi, H. Igarashi, Physica C **157**, 279 (1989).
[30]M. Paranthaman, A. Manthiram, and J. B. Goodenough, J. Solid State Chem. (to be published).
[31]J. B. Goodenough, A. Manthiram, and J. Zhou, *Proceedings of the Materials Research Society Symposium,* edited by J. B. Torrance, K. Kitazawa, J. M. Tarascon, J. D. Jorgensen, and M. Thompson (Materials Research Society, Pittsburgh, 1989), Vol. 156, p. 239.
[32]Y. Tokura, J. B. Torrance, A. I. Nazzal, T. C. Huang, and C. J. Ortiz, J. Am. Chem. Soc. **109**, 7555 (1987).
[33]J. B. Torrance, Y. Tokura, A. I. Nazzal, and S. S. S. P. Parkin, Phys. Rev. Lett. **60**, 542 (1988).
[34]K. Doverspike, J. H. Liu, K. Dwight, and A. Wold, J. Solid State Chem. **82**, 30 (1989).
[35]J. B. Goodenough, N. F. Mott, M. Pouchard, G. Demazeau, and P. Hagenmuller, Mater. Res. Bull. **8**, 647 (1973).
[36]X. X. Tang, A. Manthiram, and J. B. Goodenough, Physica C **161**, 574 (1989).
[37]J. J. Neumeier, M. B. Maple, and M. S. Torikachvili, Physica C **156**, 574 (1988).
[38]Y. Tokura, H. Takagi, and S. Uchida, Nature **337**, 345 (1989).
[39]H. Takagi, S. Uchida, and Y. Tokura, Phys. Rev. Lett. **62**, 1197 (1989).
[40]J. T. Markert and M. B. Maple, Solid State Commun. **70**, 145 (1989).
[41]E. Moran, A. I. Nazzal, T. C. Huang, and J. B. Torrance, Physica C **160**, 30 (1989).
[42]A. Manthiram and J. B. Goodenough (unpublished).

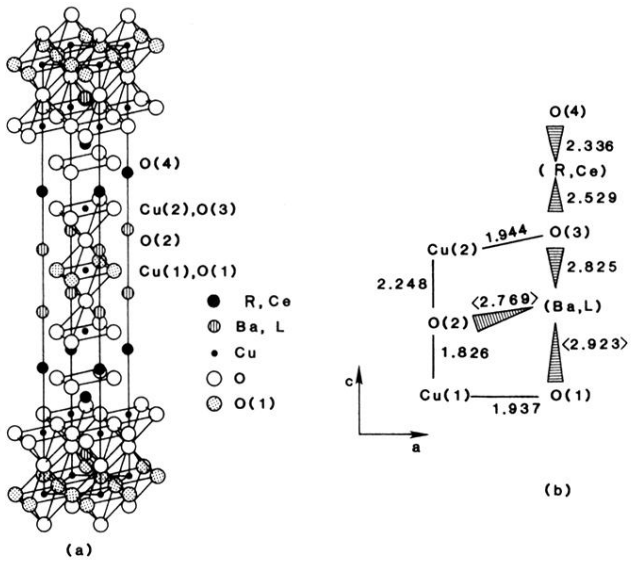

FIG. 1. (a) Crystal structure of $R_{2-z}Ce_zBa_{2-y}L_yCu_3O_{8+x}$ ($R=L=$rare earth) and (b) bond length values for $R=L=$Nd, $z=0.66$ and $y=0.73$. Adapted from Refs. 8 and 11.